nanomaterials

MDPI

Article

Nanostructure Engineering via Intramolecular Construction of Carbon Nitride as Efficient Photocatalyst for CO_2 Reduction

Muhammad Sohail [1], Tariq Altalhi [2], Abdullah G. Al-Sehemi [3], Taha Abdel Mohaymen Taha [4,5], Karam S. El-Nasser [6,7], Ahmed A. Al-Ghamdi [8], Mahnoor Boukhari [9], Arkom Palamanit [10], Asif Hayat [11,*], Mohammed A. Amin [2,*] and Wan Izhan Nawawi Bin Wan Ismail [12,*]

1 Yangtze Delta Region Institute (Huzhou), University of Electronic Science and Technology of China, Huzhou 313001, China; sohailncp@gmail.com
2 Department of Chemistry, College of Science, Taif University, P.O. Box 11099, Taif 21944, Saudi Arabia; ta.altalhi@tu.edu.sa
3 Department of Chemistry, Faculty of Science, Research Center for Advanced Materials Science (RCAMS), King Khalid University, P.O. Box 9004, Abha 61413, Saudi Arabia; agsehemi@kku.edu.sa
4 Physics Department, College of Science, Jouf University, Sakaka 75471, Saudi Arabia; themaida@ju.edu.sa
5 Physics and Engineering Mathematics Department, Faculty of Electronic Engineering, Menoufia University, Menouf 32952, Egypt
6 Chemistry Department, College of Science and Arts, Jouf University, Al-Gurayyat 77447, Saudi Arabia; karamsaif@ju.edu.sa
7 Chemistry Department, Faculty of Science, Al-Azhar University, Assiut 71524, Egypt
8 Department of Physics, Faculty of Science, King Abdulaziz University, Jeddah 21589, Saudi Arabia; agamdi@kau.edu.sa
9 College of Material Science & Engineering, Beijing University of Technology, Beijing 100081, China; bukharimahnoor11@gmail.com
10 Energy Technology Program, Department of Specialized Engineering, Faculty of Engineering, Prince of Songkla University, 15 Karnjanavanich Rd., Hat Yai, Songkhla 90110, Thailand; energy_man001@hotmail.com
11 State Key Laboratory of Photocatalysis on Energy and Environment, College of Chemistry, Fuzhou University, Fuzhou 350116, China
12 Faculty of Applied Sciences, Universiti Teknologi MARA, Cawangan Perlis, Arau Perlis 02600, Malaysia
* Correspondence: asifncp11@yahoo.com (A.H.); Mohamed@tu.edu.sa (M.A.A.); wi_nawawi@uitm.edu.my (W.I.N.B.W.I.)

check for updates

Citation: Sohail, M.; Altalhi, T.; Al-Sehemi, A.G.; Taha, T.A.M.; S. El-Nasser, K.; Al-Ghamdi, A.A.; Boukhari, M.; Palamanit, A.; Hayat, A.; A. Amin, M.; et al. Nanostructure Engineering via Intramolecular Construction of Carbon Nitride as Efficient Photocatalyst for CO_2 Reduction. *Nanomaterials* **2021**, *11*, 3245. https://doi.org/10.3390/nano11123245

Academic Editor: Otakar Frank

Received: 16 October 2021
Accepted: 18 November 2021
Published: 29 November 2021

Publisher's Note: MDPI stays neutral with regard to jurisdictional claims in published maps and institutional affiliations.

Abstract: Light-driven heterogeneous photocatalysis has gained great significance for generating solar fuel; the challenging charge separation process and sluggish surface catalytic reactions significantly restrict the progress of solar energy conversion using a semiconductor photocatalyst. Herein, we propose a novel and feasible strategy to incorporate dihydroxy benzene (DHB) as a conjugated monomer within the framework of urea containing CN (CNU-DHBx) to tune the electronic conductivity and charge separation due to the aromaticity of the benzene ring, which acts as an electron-donating species. Systematic characterizations such as SPV, PL, XPS, DRS, and TRPL demonstrated that the incorporation of the DHB monomer greatly enhanced the photocatalytic CO_2 reduction of CN due to the enhanced charge separation and modulation of the ionic mobility. The significantly enhanced photocatalytic activity of CNU–$DHB_{15.0}$ in comparison with parental CN was 85 μmol/h for CO and 19.92 μmol/h of the H_2 source. It can be attributed to the electron–hole pair separation and enhance the optical adsorption due to the presence of DHB. Furthermore, this remarkable modification affected the chemical composition, bandgap, and surface area, encouraging the controlled detachment of light-produced photons and making it the ideal choice for CO_2 photoreduction. Our research findings potentially offer a solution for tuning complex charge separation and catalytic reactions in photocatalysis that could practically lead to the generation of artificial photocatalysts for efficient solar energy into chemical energy conversion.

Keywords: carbon nitride (CN); dihydroxy benzene (DHB); photocatalysis; copolymerization; CO_2 reduction

1. Introduction

The production of renewable fuels with rich CO_2 as raw materials through solar energy has been considered the best solution for energy crises and environmental remediations [1–5]. It is always attracting and has received much attention for generating renewable fuel from the conversion of CO_2 through semiconductor-based photocatalysts [5–8]. To date, a variety of semiconductor photocatalysts including CeO_2, TiO_2, Ga_2O_3, ZnO, $ZnGe_2O_4$, and Bi_2WO_6 have been used for the reduction of CO_2 source [9–15]. Unfortunately, such semiconductor materials have a broad bandgap that absorbs only ultraviolet light irradiation and has less photocorrosion potential. Furthermore, bulk semiconductors typically have a high recombination rate of photoinduced charge carriers [16,17]. All of these disadvantages substantially jeopardize the effectiveness and successful long-term implications of CO_2 photoconversion on the basis of photocatalysts. As a result, it is vital for photocatalytic CO_2 conversion to fabricate and construct visible light-responsive, highly efficient, and durable catalysts [5,18,19]. Numerous strategies, such as morphological tailoring, junction creation, crystal facet engineering, and surface modification, can be used to prevent the recombination of highly reactive photogenerated carriers in photocatalysis. Despite this, the photocatalytic performance is limited due to a lack of active sites and photocorrosion features. The proper coupling of one semiconductor with other materials to form a heterojunction may aid in the separation of spatial charges and protect the light-harvesting semiconductor from photocorrosion [20–22].

Numerous articles have been published about heterogeneous photocatalysis since 1981, demonstrating the topic's increasing popularity [23]. The heterogeneous catalyst has a well-defined structure, and the reaction is multi-sited, involving multiple active sites such as edge, face, and defect simultaneously [24]. Photocatalytic materials such as metal oxides, sulfides, and nitrides have been studied in the literature widely [25]. CdS is a semiconductor with a bandgap of 2.42 eV and an absorption peak of 514 nm. Consequently, CdS is more effective at absorbing visible light or UV radiation with a wavelength of less than 514 nm [26]. Aside from water decomposition [26] and CO_2 reduction [27], CdS semiconductors have a bandgap location that is ideal for several photocatalytic processes. Furthermore, the CdS conduction band edge is lower than the other common semiconductors (such as TiO_2, $SrTiO_3$, and ZnO [28]), which means that photoelectrons of CdS have a stronger reducing power in the photocatalytic reaction. As a result, the photocatalytic properties of CdS have been extensively studied. However, the CdS material is susceptible to light corrosion, which limits the number of photocatalysts that can be restored.

Carbon nitride (CN) has received considerable attention as a metal-free organic semiconductor due to its remarkable thermal and chemical stability and favorable electrical structure [29–35]. CN has been shown to be a potential solar energy conversion candidate [36,37]. The synthesis of bulk CN by the direct co-condensation process limits their applications because of its low surface area and less active site [13,34,38–40]. To improve the quantum efficiency in the visible light region, the above-mentioned drawbacks must be overcome that limit the applications of CN [35,41]. The fabrication of hierarchical micro/nanostructures is an effective method for addressing these issues. Micro/nanostructured CN was obtained using a variety of techniques, including hard templating, which was commonly used to obtain porous, sphere, and tubular carbon nitride (CN) [13,39]. However, the templating technique is expensive, time-intensive, and not eco-friendly, given the environmentally toxic reagents to be used for the extraction of the prototype, which prevents further functionalization. A variety of techniques have been used to modify CN, including doping, morphology tailoring in the form of nanorods, and hollow nano-spheres junction fabrication, crystal facet engineering, and surface modification [5,42–44]. Inspired by these advancements, molecular engineering (copolymerization) has arisen as a new significant technique by incorporating new energetic organic conjugated monomers within the framework of CN to improve its photocatalytic properties [5,33,37,39,43,44]. Incorporating these organic motifs into the CN structure via copolymerization enhances photogenerated electron accumulation and transport, leading

to improved photocatalytic activity under visible light irradiation [5,33,37]. To achieve high photocatalytic efficiency and stability, this copolymerization grafts organic motifs within the CN skeleton by using a simple one-step condensation technique [42]. From the perspective of this approach, Nie et. al. developed Z-scheme g-C_3N_4/ZnO microspheres for CO_2 reduction [45]. Hasija et al. designed Z-scheme g-C_3N_4/AgI/ZnO/CQDs photocatalysts for the efficient photodegradation of 2,4-dinitrophenol, which exhibited remarkable stability and recyclability [21]. Hayat et al. examined the introduction of trimesic acid as a conjugated co-monomer within the CN framework that was highly effective in photocatalytic CO_2 reduction [5,18]. Intramolecular conjugating monomers are of great interest and are discovered as energized candidates for intramolecular donor–acceptor behaviors within the triazine subunit of CN to boost its photocatalytic activity [42]. CN has been employed for CO_2 photoreduction by several groups due to its large surface area and distinct semiconductor properties [46,47]. These features may lead to the formation of charge carriers capable of activating CO_2 molecules at the active sites of the nitrogen-rich CN skeleton. Liu et al. demonstrated the synthesis of layered heterojunction photocatalysts (PCN/$ZnIn_2S_4$) via the in situ growth of 2D $ZnIn_2S_4$ nanosheets on the surfaces of ultrathin CN layers for improved CO_2 conversion under visible light [48]. In addition, the CN/$ZnIn_2S_4$ composites also demonstrate enhanced photoactivity for deoxygenated CO_2 conversion. On the other hand, Xue et al. [49] proposed a new strategy for solar fuel production with simultaneous organic synthesis using photo-holes oxidation power on amphiphilic metal-free semiconductors. The successfully grafted pyrene functional group onto the CN surface via a post copolymerization technique (Py-CN) shows unique biphasic photocatalytic activities that allow efficient CO_2 photoreduction in aqueous solution while effectively oxidizing alkenes (C=C) in the organic phase. This is due to the pyrene functional group enhanced lipophilicity, allowing hydrophobic alkene molecules to reach the CN surface and react with hydroxyl radicals (OH) produced by photogenerated holes [50].

In the present work, we use urea containing CN to introduce hydroxyl groups containing benzene rings, i.e., 1,4-dihydroxybenzene organic conjugated monomer (DHB) through copolymerization and studied the versatile application of products for photocatalytic CO_2 reduction. The incorporation of an aromatic benzene ring into the triazine analogous of CN can produce a regular inner structure of CN as a spinal candidate to achieve a polymeric conjugated C–N network system. The aromaticity of the benzene ring in the CN framework can improve the photo-excitation process of electrons from the ground state to the excited state, as well as photogenerated charge separation. As discussed above, the integrated monomer into the CN skeleton will be either an electron donor or an acceptor; therefore, the dihydroxybenzene monomer acts as an electron donor. Figure 1 provides a proposed reaction mechanism for the incorporation of dihydroxybenzene (DHB) into the CN framework by donating electrons to the pristine CN to make a long polymer network that has high stability and a large surface area. An as-synthesized sample showed good photocatalytic activity of CO_2 reduction into CO and H_2 sources, which was roughly 4-fold higher than the parental CN. This effort will open up new possibilities to promote the use of copolymerized CN for CO_2 photofixation under visible illumination.

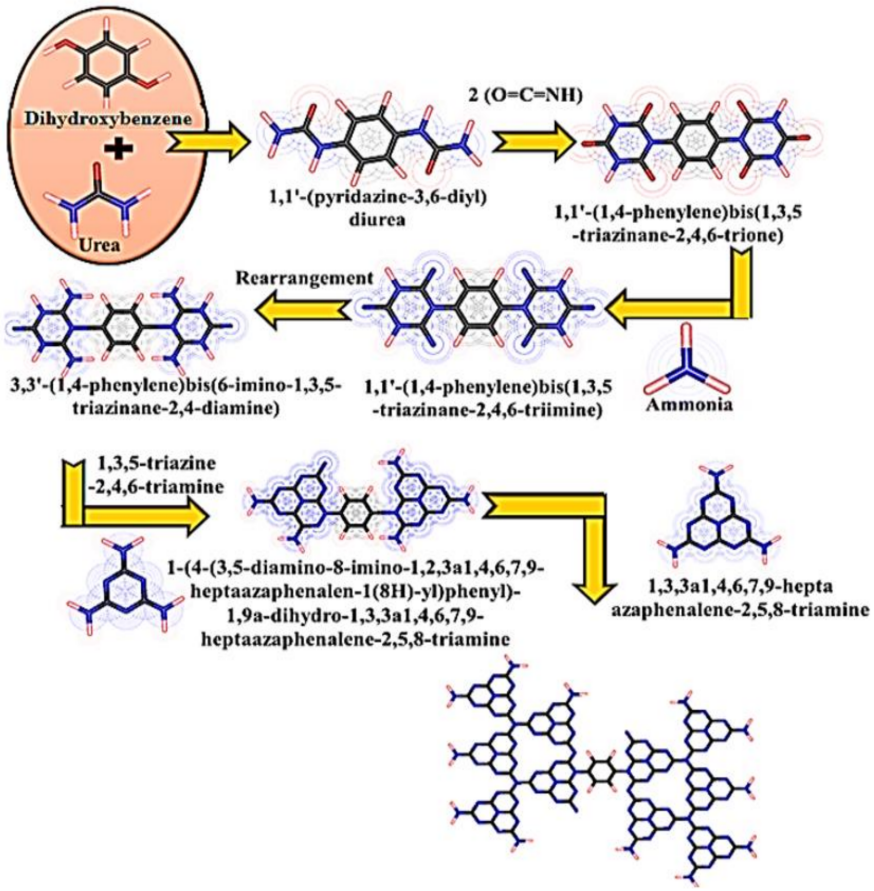

Figure 1. Proposed reaction mechanism of incorporating dihydroxybenzene (DHB) into CN networks.

2. Experimental

Synthesis of CN and Copolymerized CN Photocatalysts

A pristine CN sample was prepared by taking a specific amount of urea as a precursor in a 30 cm × 60 cm rectangle crucible dish, and the resulting product was annealed at 550 °C in an air furnace for 2 h at a heating rate of 4.5 °C min^{-1}. After calcinations, the yellow color sample is obtained and labeled as CNU (U denotes the urea containing carbon nitride). Similarly, the copolymerized samples were synthesized by taking 10 g of urea with varied amounts of 1,4-dihydroxybenzene (DHB) monomer in 15 mL distilled in an oil bath system by heating at 100 °C through vigorous stirring to remove water thoroughly. After the evaporation of water, the solid samples were transferred into a 30 cm × 60 cm rectangle crucible one by one and heated for 2 h at 550 °C at a 4.5 °C min^{-1} rate. After heating, various color-containing samples were obtained depending on the amount of DHB monomer to be copolymerized. The as-prepared samples were marked as CNU-DHBx where x determines different amounts of DHB to be copolymerized with carbon nitride (x = 0.0050, 0.0100, 0.0150, 0.0200, 0.0250, 0.0300 g), respectively. Up to a specific amount of DHB with CNU, the color of the samples was obtained from dark yellow to brown. All prepared samples were characterized for different techniques without any further purification or washing.

3. Result and Discussion

As-synthesized samples of pristine and copolymerized CN samples were characterized by employing the X-ray diffraction (XRD) technique [39,51,52]. Figure 2a demonstrates that there are no extra peaks observed in the XRD of pristine CNU and copolymerized CNU-DHBx, respectively. All samples had two distinct peaks, and the evidence indicated the same structural composition; thus, no detection of extra impurity peaks was observed.

The peak at 12.9° indexed as (1 0 0) for all samples represents the inter-layer distance in the structural repeating unit of triazine motifs. The distance between these repeating units is approximately 0.68 nm. A dominant peak at 27.7° (0 0 2) is due to the periodic interlayer stacking of the conjugated aromatic system of CN at 0.32 nm. This periodic stacking distribution in the conjugated system of CN could be determined from the integration of DHB monomer within the skeleton of CNU. For as-synthesized samples, FTIR spectroscopy was used to determine the chemical composition of all samples [39,53]. Figure 2b illustrates the stretching and bending vibration of the heptazine ring unit, which is assigned from several peak locations of the absorption bands at 810 cm^{-1} and 1200–1630 cm^{-1}, respectively. All of the prepared samples have one common broad peak, which is located between 3000 and 3600 cm^{-1} and attributed to the stretching modes of the O–H and N–H groups, which confirms the presence of the amino and hydroxyl group that originated from the condensation process. Another peak located at 1200 to 1600 cm^{-1}, which is due to the breathing mode of 810 cm^{-1} triazine units, is quite similar to that of CNU. The XRD and FTIR analysis demonstrate that pristine CNU and copolymerized CNU-DHBx have similar a phase composition and chemical structure. Thus, the incorporation of a DHB monomer in the framework of CNU does not carry any change in the crystal and chemical integrity structure of CNU [39,42].

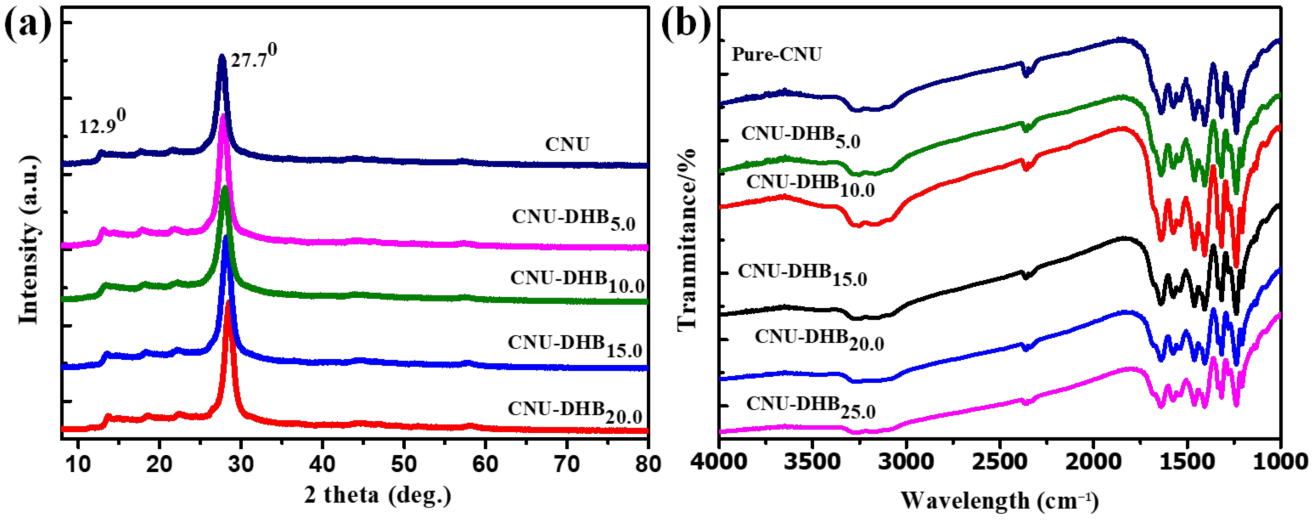

Figure 2. (**a**) XRD spectrum and (**b**) FTIR spectra of CNU and CNU–DHBx samples.

Similarly, the induction of conjugated DHB within the skeleton of CN alters several changes in the chemical analysis of CN that can be confirmed from solid-state ^{13}C NMR spectra and XPS analysis, respectively. The XPS survey spectra were investigated to figure out the chemical composition states within samples. Figure 3a,b demonstrate the XPS wide spectrum for parental CNU and copolymerized CNU-$DHB_{15.0}$ samples mainly composed of carbon (C), nitrogen (N), and oxygen (O), respectively. The O1 s peak detected at 533 eV for both CNU and CNU-DHBx arises due to the adsorption of atmospheric moisture during synthesis. High-resolution XPS spectra of C 1s for CNU-$DHB_{15.0}$ and CNU composed of two distinct peaks are altered; a small shifting occurs in the perception of peaks indexed at 284.3 eV for CNU and 284 eV for CNU-$DHB_{15.0}$, which is attributed to the sp^2 C–C bonds (Figure 3c,d). However, the other peak indexed at 287.5 eV for CNU and at 288 eV for CNU-$DHB_{15.0}$ ascribed the sp^2 hybridized carbon located in the cage of the N-containing aromatic ring (N–C=N). Furthermore, the high-resolution XPS spectra of N 1s also alters the shifting of peaks de-convoluted into four peaks. The main peak centering at 398 eV for CNU and 398.7 eV for CNU-$DHB_{15.0}$ corresponds to the sp^2 hybridized nitrogen within the carbon (C−N=C). Hence, the other peaks indexed at 398.8, 400.3, and 403.8 eV for CNU and 399.7, 401.2, and 404.3 eV for CNU-$DHB_{15.0}$ display the bridging tertiary nitro-

gen (N–$(C)_3$), graphitic N, and amino functional groups (C−N−H) [39,42], as illustrated in Figure 3e,f.

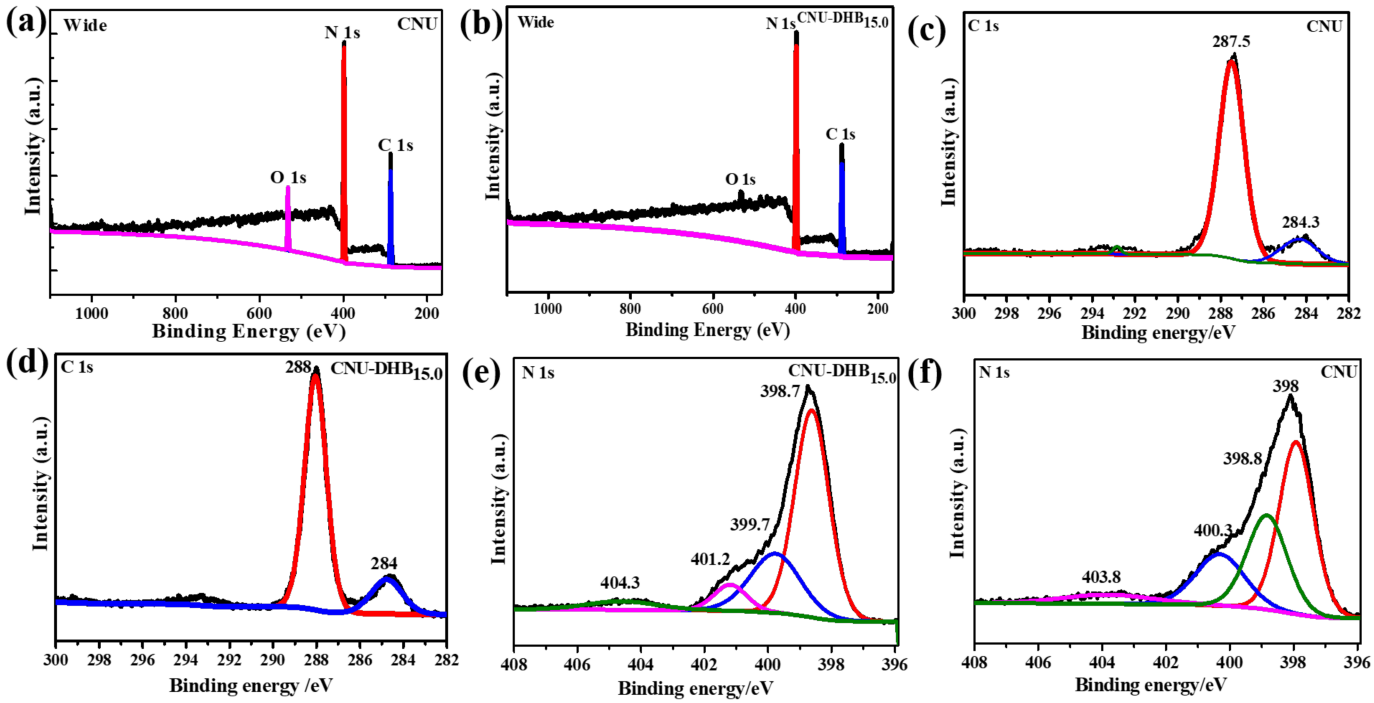

Figure 3. (**a**,**b**) Wide spectrum, (**c**,**d**) C 1s, and (**e**,**f**) N 1s high-resolution XPS spectra of the CNU–$DHB_{15.0}$ and CNU samples.

The solid-state ^{13}C NMR spectra for CNU and CNU-$DHB_{15.0}$ samples were used to examine the extra evolution of carbon contents after the copolymerization process (Figure S1). All of the peak alignments in the NMR spectra for both samples are the same, but a new peak was indexed at 135.7 ppm for the CNU-$DHB_{15.0}$ sample, thus confirming the increased amount of carbon. The morphology and microstructure of pure CNU and CNU-$DHB_{15.0}$ were analyzed by FESEM and TEM, as illustrated in Figure 4. The FESEM morphology of pure CNU obviously demonstrates an agglomerated shape having irregular small stacking flakiness, as displayed in Figure 4a,b, while this morphology became elongated in size after the inducing of a DHB monomer within CNU, having a large cloudy superficial area, as shown in Figure 4c,d. The typical TEM images of pure CNU (Figure 4e,f) and CNU-$DHB_{15.0}$ (Figure 4g,h) exhibit platelet ribbon-like distorted morphology for pure CNU samples. After copolymerization, the surface morphology become dense, stacked, and proliferous, which results in an increase in the surface area.

The UV-Vis diffuse reflectance spectroscopy (DRS) of the samples was used to assess the effect of the DHB monomer on the optical property of CNU, as shown in Figure 5a. After DHB incorporation into the backbone of CNU, the optical bandgap is significantly reduced, which facilitates the harvesting of light and photogenerated carriers [39,42]. To study the transfer and exciton separation behavior of the photogenerated electrons and holes of the as-prepared copolymerized samples, we carried out photoluminescence (PL) spectra at room temperature under 370 nm excitation (Figure 5b). All these samples show a wide broad peak indexed at around 455 nm and extend their tail to 600 nm. The spectra demonstrate two types of band: i.e., a shoulder band, which is attributed to the emission process of CN from the valence band (LUMO) toward the conduction band (HOMO) at a shorter wavelength of 440 nm. The other PL band corresponds to the emission of charges as found in donor–acceptor polymers [54]. Actually, in CNU, the weak shoulder band is produced due to the emission of charges at about 463 nm. Similarly, the rates of transfer of photogenerated charges toward transition states are much higher in copolymerized samples compared to pristine samples. To understand the exciton separation behavior, we

conducted surface photovoltage. When compared to the copolymerized sample, pristine CNU exhibits a weak SPV signal at 350–550 nm (Figure 5c), which is due to the low charge separation compared to pristine. Nonetheless, the copolymerized CNU exhibits a clear enhancement of the SPV signal, indicating an increased charge separation due to the aromaticity of the benzene ring in the CN framework, which acts as an electron-donating species. The effect of the aromaticity of the benzene ring of DHB in the framework of CN, acting as an electron-donating species, was further verified by OCP spectra, as shown in Figure 5d. The C/N ratio and bandgap for all of the as-synthesized samples are depicted in Table S2, in which the superior sample CNU-DHB$_{15.0}$ demonstrates a boosted C/N ratio and low bandgap, respectively.

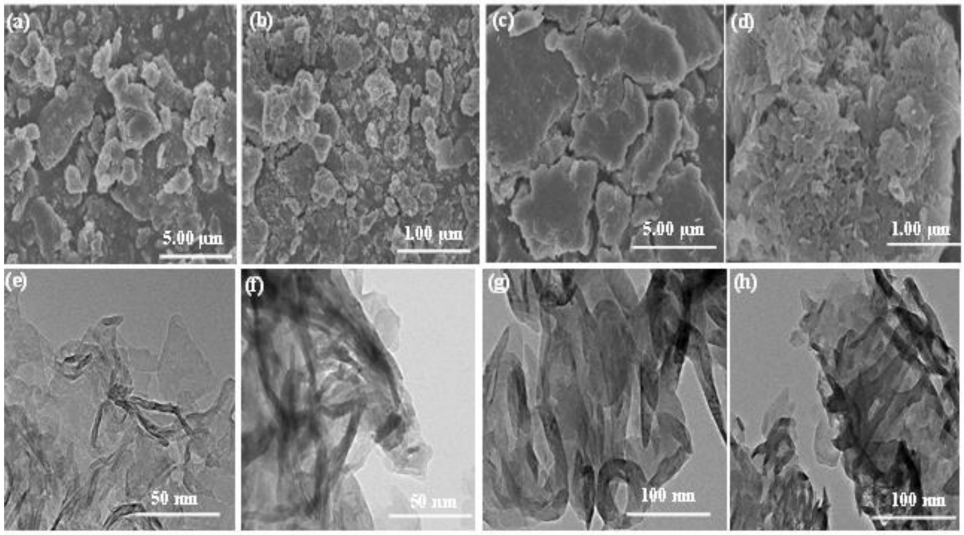

Figure 4. FESEM of CNU (**a**,**b**) and CNU–DHB$_{15.0}$ (**c**,**d**), TEM images of CNU (**e**,**f**) and CNU–DHB$_{15.0}$ (**g**,**h**).

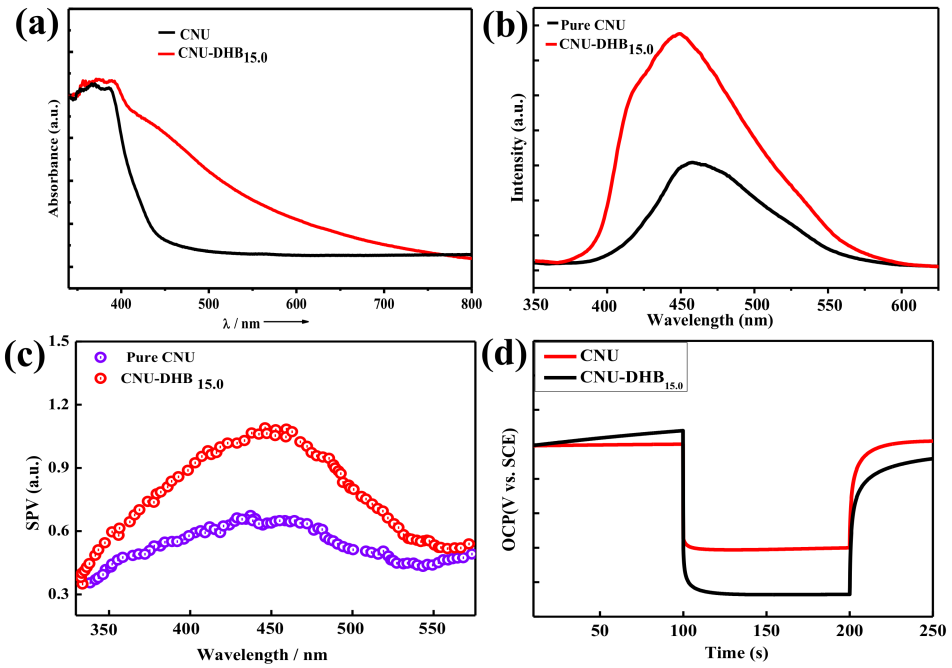

Figure 5. (**a**) UV-Vis DRS spectra of the CNU and CNU–DHBx samples under 370 nm excitation. (**b**) The photoluminescence spectrum of the CNU and CNU–DHBx samples at room temperature. (**c**) SPV spectra of the CNU and CNU–DHBx samples. (**d**) OCP response curve of the CNU and CNU–DHBx samples.

The Brunauer–Emmett–Teller (BET) method was conducted to examine the specific surface area of as-synthesized samples (Figure 6a). Both samples (CNU and CNU-$DHB_{15.0}$) represent the N_2 adsorption–desorption isotherms having H_3 hysteresis-type loops [55]. The surface area of blank CNU is 49.9 m^2/g and after the copolymerization process, the surface area of CNU-$DHB_{15.0}$ improved to 123.7 m^2/g, respectively. Actually, large surface areas supply an abundance of energized sites for the photocatalytic reaction that result in photocatalytic performance. Figure 6b illustrates the BJH pore size distribution and highlights that the catalysts' pore size decreases and pore volume increases, hence originating the structure of samples as mesoporous. Actually, during the co-condensation process of samples, various gases evolved from their partial decomposition and adopted mesoporous structures [39,42]. The CO_2 adsorption isotherm was evaluated for pristine CNU and copolymerized CNU-$DHB_{15.0}$, as illustrated in Figure 6c, indicating that CNU-$DHB_{15.0}$ has remarkable CO_2 adsorption ability compared to pure CNU. The surface area for all of the as-synthesized samples was depicted in Table S2, in which the superior sample CNU-$DHB_{15.0}$ demonstrates a high surface area.

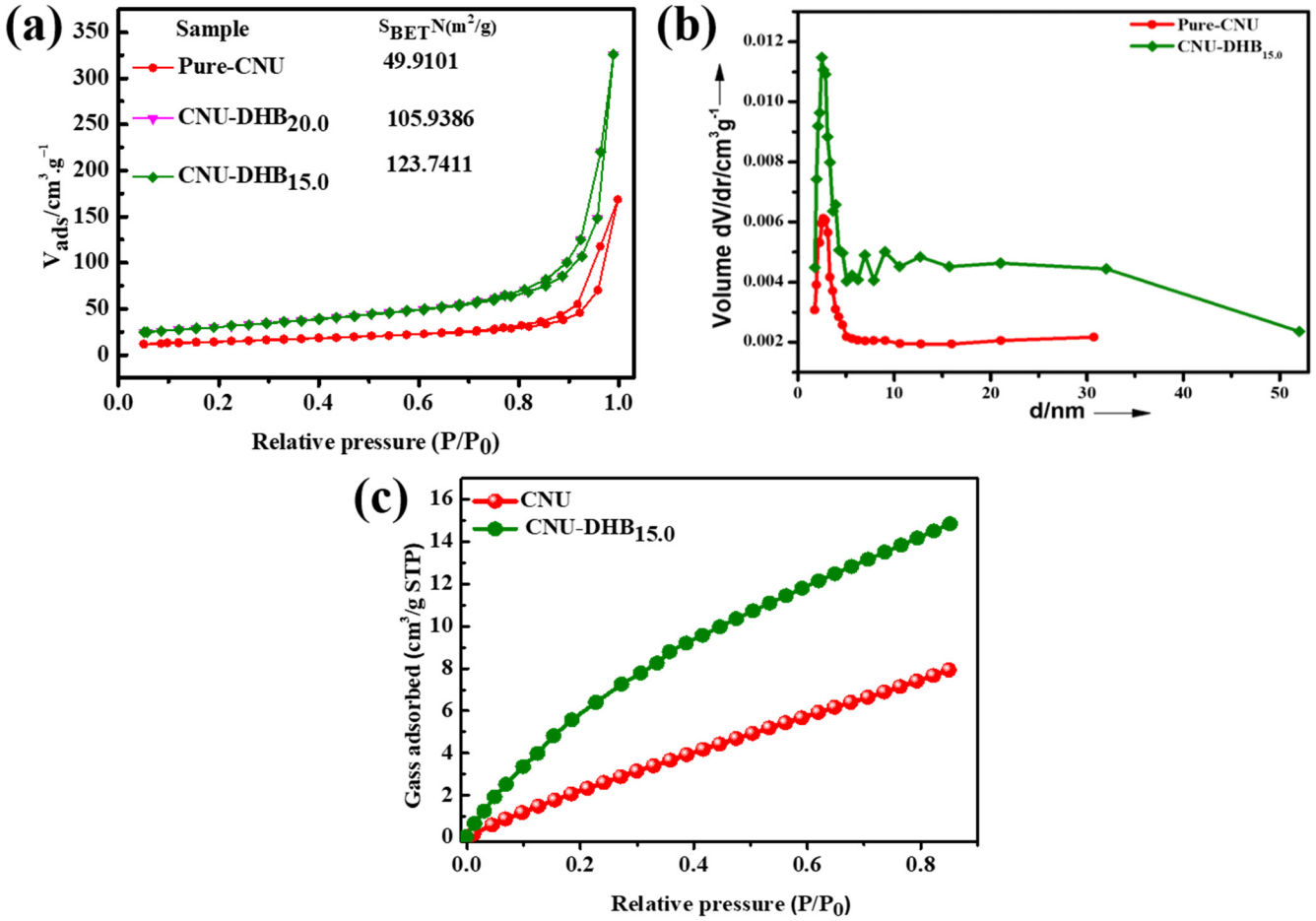

Figure 6. (**a**) N_2 adsorption–desorption isotherms (77 K), (**b**) BJH pore size distribution, and (**c**) CO_2 adsorption isotherms (273 K) for CNU and CNU-$DHB_{15.0}$ samples.

The photocatalytic activity of CO_2 reduction was carried out under visible light illumination ($\lambda > 420$ nm). Typically, 30 mg of photocatalyst was dispersed in a solvent (MeCN)/H_2O = 5:1) containing $Co(bpy)_3Cl_2 \cdot 6H_2O$ as a photosensitizer and triethanolamine (TEOA) as a sacrificial electron donor [18]. The reactions were carried out for half an hour to five hours, generating a significant amount of CO (32.5 $\mu mol/h^{-1}$) in the first hour and achieving a high CO efficiency, i.e., 85 $\mu mol/h$ in five hours (Figure 7a). Similarly, bulk CNU photocatalysts have poor photocatalytic performance compared to

CNU-DHB$_{15.0}$. The photocatalytic reduction of CO_2 was enhanced after the incorporation of DHB in the framework of CNU, indicating the best activity in optimal condition (Figure 7b). All of the other copolymerized samples demonstrate good photocatalytic performance and are much better than pristine CNU. In all of these photocatalysts, CNU-DHB$_{15.0}$ manifested a boosted performance for the photocatalytic CO_2 reduction under visible light (Table S2). Similarly, the activity of samples decreases due to the appearance of a negative site from the excess amount of DHB monomer that destroys the conjugated system of CN. Figure 7c demonstrates the recycle stability of the CNU-DHB$_{15.0}$ photocatalyst, which depicts a high photocatalytic stability toward CO_2 reduction in every phase. The long durability experiments demonstrate a decline in the few cycles, which is correlated with the erosion of the co-catalyst cobalt due to the long interaction of solar light during a reaction.

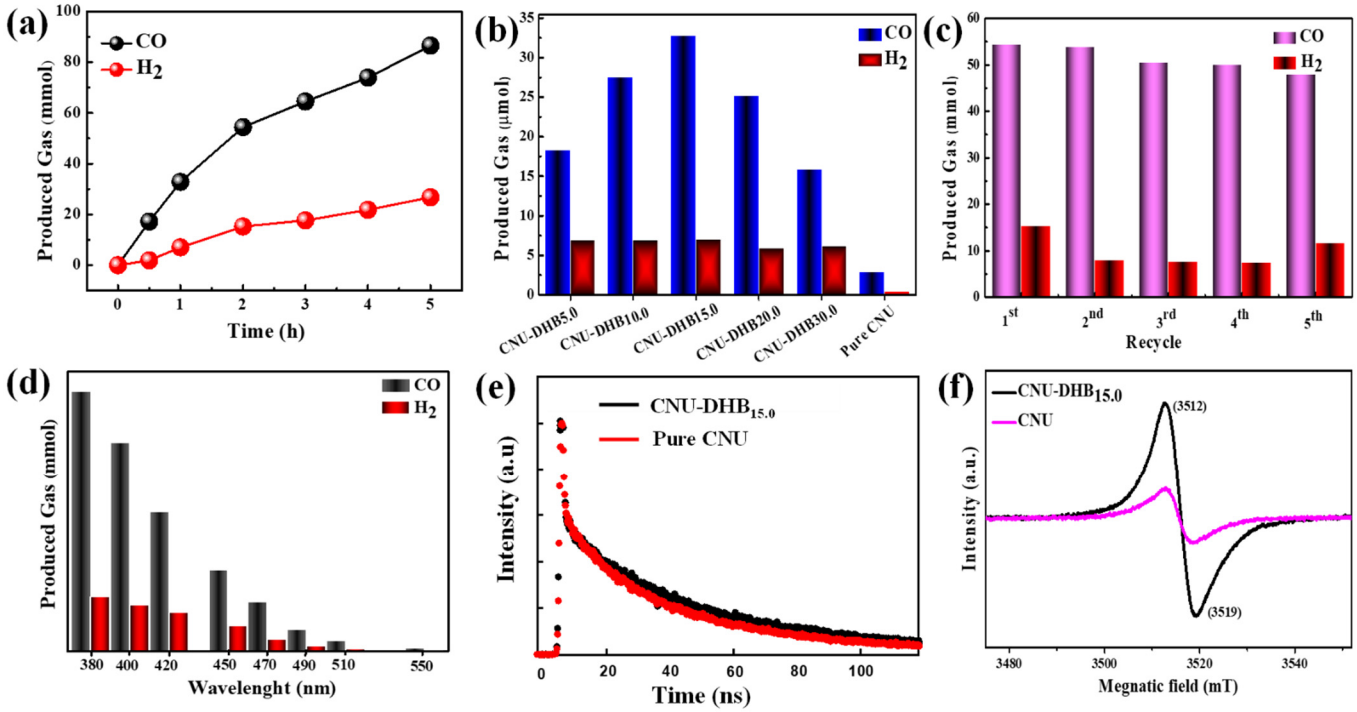

Figure 7. Reduction (**a**) Time-production plot between CNU and CNU-DHB$_{15.0}$, (**b**) Comparison of photoreduction with different photocatalysts synthesized, (**c**) Recycling stability test, (**d**) Different wavelength experiments, (**e**) TRPL spectra of CNU-DHB$_{15.0}$ and pure CNU, (**f**) EPR spectra of CNU and CNU-DHB$_{15.0}$.

Long-range wavelength experiments have been conducted for the superior sample CNU-DHB$_{15.0}$ to investigate the effect of light source on the photocatalytic products (Figure 7d). The results manifest that the light of a longer wavelength decreases the photocatalytic evolution of CO and H_2, suggesting that light-harvesting phenomena is responsible for the CO_2 photoreduction by generating stimulated electrons [18]. The EPR and life time spectra of as-synthesized samples were conducted, as demonstrated in Figure 7e,f. The life time decay of superior sample is much enhance than the blank samples and same the EPR peak intensity of the CNU-DHB$_{15.0}$ sample improved and broadened immediately as compared to pristine CNU. Upon copolymerization, the unpaired electrons of carbon atoms increase the EPR peak intensity and also increase the delocalization of π-conjugated clusters. Most photochemical radical pairs generate light on the catalyst surface by trapping it under visible light [56–58]. A comparison of the reported results of the photocatalytic CO_2 reduction with our current research work is presented in Table S1.

Similarly, several isotopic controlled experiments were held using $^{13}CO_2$ as feedback to analyze the insights of carbon contents of the produced carbon monoxide (CO) products under similar conditions. After irradiation of one hour, the gas chromatography and mass

spectrometry (GC-MS) demonstrate that the peak produced at 2.4 mint having m/z = 29 originated due to the reactant of $^{13}CO_2$, as illustrated in Figure 8a,b. The result strongly suggests that photocatalytic CO_2 reduction into the CO product is absolutely performed by using the original reactant CO_2 gas.

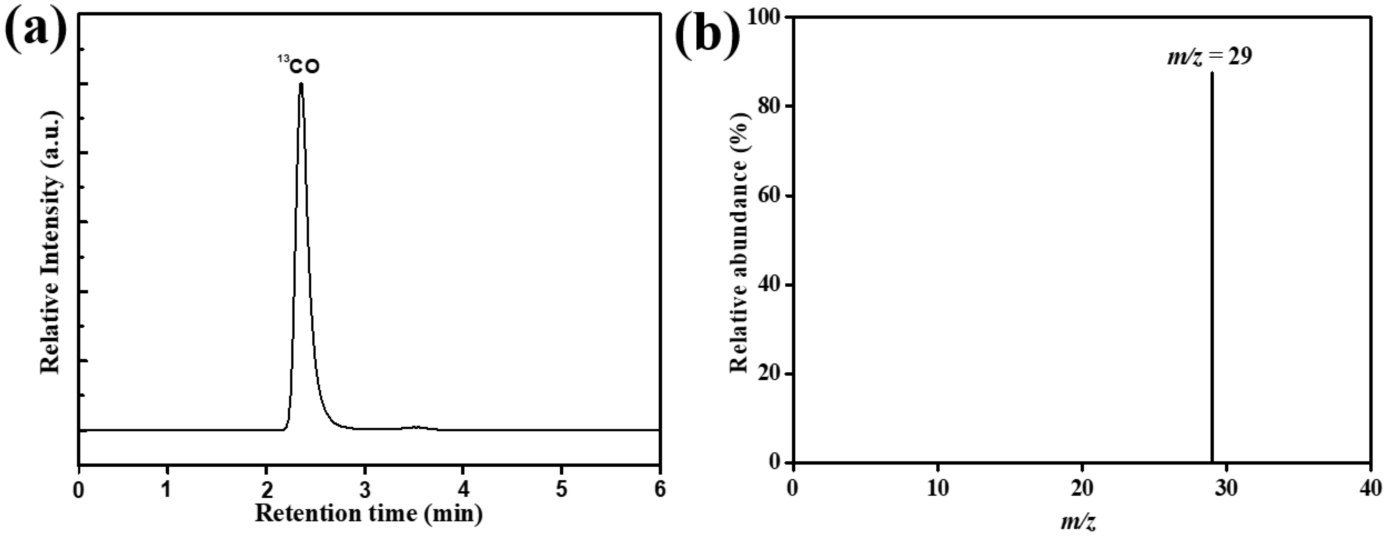

Figure 8. (**a**) Gas chromatogram and (**b**) mass spectrum analysis of the carbon products using CNU-DHB$_{15.0}$ as catalyst and $^{13}CO_2$ as reactant.

The photocatalytic activities of the synthesized samples were evaluated for the degradation of rhodamine B under visible light irradiation (λ = 420 nm), as shown in Figure S2a. The CNU-DHBx catalyst shows better photocatalytic activities than pure CNU. The degradation rate of rhodamine B is enhanced after the copolymerization process. Similarly, few experiments for the degradation of RhB were conducted under dark illumination, and no noticeable photodegradation activity was observed, so it was concluded that the reaction and catalysts are only active under visible light illumination. The overall degradation was carried out for 70 min under visible light at varying exposure times. The kinetic of RhB degradation using the CNU-DHB$_{15.0}$ photocatalyst (Figure S2b) was performed successfully and was calculated with a pseudo-first-order equation as fellows.

$$\ln (C_0/C) = kt \quad (1)$$

where the apparent rate constant of the pseudo-first order is shown in the above Equation (1) k, the time of irradiation applied during the degradation process shall be t, and the initial and final concentration of the RhB solution shall be C_0/C [16]. The result confirms that CNU-DHB$_{15.0}$ has a better kinetic rate constant value and also investigates the pseudo-first-order catalytic rate constants from the slope of the plots, which are four times higher than that of pure CNU. The apparent rate constants for RhB degradation through different synthesized samples are depicted in Figure S2c. The recycling experiments were conducted for the superior photocatalyst CNU-DHB$_{15.0}$ in order to check its stability toward the photodegradation of RhB. Figure S2d shows the cyclic stability experiments for the RhB, and for this function, the used CNU-DHB$_{15.0}$ catalysts were centrifuged, washed several times with ethanol and water, and dried to reuse in a fresh reaction. The results reveal that CNU-DHB$_{15.0}$ showed good photocatalytic activity and stability in practically all of the four cycling runs, and hence, no obvious decline was observed after long-term use. It indicates that CNU-DHBx is highly stable and can be reused for the treatment of RhB.

4. Photocatalytic Mechanism

The possible scheme for the photocatalytic H_2 production and CO_2 with the CNU-$DHB_{15.0}$ photocatalyst was evaluated, as shown in Figure 9. When irritated under solar light, the electrons are excited to the conduction band (CB), leaving positive holes in the valence band (VB) of the CNU-$DHB_{15.0}$ photocatalyst. The excited electrons in the CB of CNU-$DHB_{15.0}$ reduce protons to reduce CO_2 into the CO source, while the positive holes in the VB contribute to oxidizing TEOA. The particles of cobalt (CO) play an important role in the separation of exited charges through its metallic character called surface catalysis. In the reaction system, the small addition of catalysts with solvent creates splits on the interface of material; then, H^+ ions are produced, which trap the electrons and generate H_2 fuel. Although a large number of the photoelectrons and holes produced are attributed to the absorption of solar photons, a very small portion of these charges is used for effective photocatalysis. To accelerate the photocatalytic production of H_2 fuel, the separation of electrons and holes through CO and sacrificial agent TEOA is very important. Similarly, the induced holes in the VB of the superior sample results are oxidized, which participate in the photocatalytic degradation of RhB reduction under visible light illumination (λ = 420 nm).

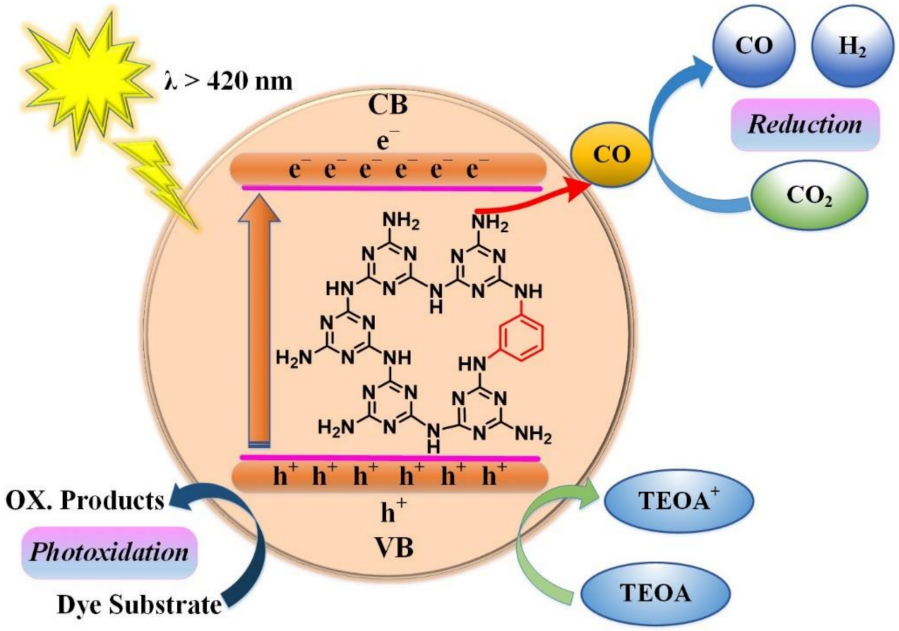

Figure 9. The proposed reaction mechanism for photo reduction and degradation through CNU-$DHB_{15.0}$.

5. Conclusions

The modification of carbon nitride (CNU) for photocatalytic CO_2 reduction is an enticing research topic owing to the growing severity of fuel and ecological ailments. In this study, the organic aromatic co-monomer dihydroxybenzene (DHB) was thermally incorporated within carbon nitride (CNU referred to as urea-based carbon nitride) through the copolymerization process recognized as CNU-DHB. Interestingly, the copolymerized samples demonstrated an efficient CO_2 reduction due to the aromaticity conjugated π electrons of the benzene ring in the framework of CN, which acts as an electron-donating species; therefore, it can speed up the process of photogenerated charge separation. This assimilation altered a significant change in the electronic structure of CNU, boosted its electron transport, and increased the photocatalytic properties of CNU under visible light irradiation. The CNU–$DHB_{15.0}$ catalyst yielded 85 μmol/h of CO and 19.92 μmol/h of H_2 source after 5 h of irradiation, highlighting the maximum yield of photocatalytic performance that is almost four times higher than that of parental CNU. Such an approach predicts a substantial distraction in the precise surface area, energy gap, and chemical

properties, and it promotes the effective segregation of photoinduced load carriers from HUMO toward LOMO of CNU, making it an ideal alternative for photocatalytic CO_2 reduction reactions. Thus, the CNU-$DHB_{15.0}$ composite photocatalyst provides a useful guide for the synthesis of efficient photocatalysts for photocatalytic applications.

Supplementary Materials: The following are available online at https://www.mdpi.com/article/10.3390/nano11123245/s1, Figure S1: Solid-state ^{13}C NMR spectra of pure CNU and CNU-$DHB_{15.0}$ samples. Figure S2: (a) Visible light photocatalytic degradation (b) first-order kinetics data (c) the apparent rate constants for RhB degradation (d) Cycling runs of CNU-$DHB_{15.0}$ catalyst for the photocatalytic degradation of rhodamine (RhB) dye (λ = 420 nm) Table S1: comparison of photocatalytic performance of CO_2 reduction. Table S2: Different parameters of our synthesized photocatalysts.

Author Contributions: M.S. have performed the experiments, data analysis and article writing, T.A., T.A.M.T., A.G.A.-S., K.S.E.-N. and A.A.A.-G., collaborated investigation and give a data curation. M.B. and A.P. review and editing paper. A.H., M.A.A. and W.I.N.B.W.I., done visualization, supervision, project administration. All authors have read and agreed to the published version of the manuscript.

Funding: We gratefully acknowledge the support of this research by funding from the Foundation of Yangtze Delta Region Institute (Huzhou) of UESTC, China, (Nos. U03210057). The authors are also grateful to the Taif University Researchers Supporting Project number (TURSP-2020/03), Taif University, Taif, KSA. The authors acknowledge the support and funding of King Khalid University; grant no: KKU/RCAMS/006/21. Finally, the authors would like to thank the Ministry of higher education, Malaysia (MOHE) for providing financial support under PRGS grants: (PRGS/1/2021/STG04/UITM/02/1), Universiti Teknologi MARA (UiTM).

Institutional Review Board Statement: Not applicable.

Informed Consent Statement: Not applicable.

Data Availability Statement: The data presented in this study are available on request from the corresponding author.

Conflicts of Interest: The authors declare no conflict of interest.

References

1. Listorti, A.; Durrant, J.; Barber, J. Artificial photosynthesis: Solar to fuel. *Nat. Mater.* **2009**, *8*, 929–930. [CrossRef]
2. Hori, Y. *Electrochemical CO_2 Reduction on Metal Electrodes*; Springer: New York, NY, USA, 2008.
3. Hamid, A.; Khan, M.; Hayat, A.; Raza, J.; Hussain, F. robing the physio-chemical appraisal of green synthesized PbO nanoparticles in PbO-PVC nanocomposite polymer membranes. *Spectrochim. Acta Part A Mol. Biomol. Spectrosc.* **2020**, *235*, 118303. [CrossRef]
4. Centi, G.; Perathoner, S. *Perspectives and State of the Art in Producing Solar Fuels and Chemicals from CO_2. Green Carbon Dioxide: Advances in CO2 Utilization*; Wiley Online Library: Hoboken, NJ, USA, 2014; pp. 1–24.
5. Hayat, A.; Khan, J.K.; Rahman, M.U.; Mane, S.B.; Khan, W.U.; Sohail, M.; Rahman, N.U.; Shaishta, N.; Chi, Z.; Wu, M. Synthesis and Optimization of the Trimesic Acid Modified Polymeric Carbon Nitride for Enhanced Photocatalytic Reduction of CO_2. *J. Colloid Interface Sci.* **2019**, *548*, 197–205. [CrossRef] [PubMed]
6. Sato, S.; Morikawa, T.; Saeki, S.; Kajino, T.; Motohiro, T. Visible-light-induced selective CO_2 reduction utilizing a ruthenium complex electrocatalyst linked to a p-type nitrogen-doped Ta_2O_5 semiconductor. *Angew. Chem.* **2010**, *122*, 5227–5231. [CrossRef]
7. Kuriki, R.; Matsunaga, H.; Nakashima, T.; Wada, K.; Yamakata, A.; Ishitani, O.; Maeda, K. Nature-Inspired, Highly Durable CO_2 Reduction System Consisting of a Binuclear Ruthenium(II) Complex and an Organic Semiconductor Using Visible Light. *J. Am. Chem. Soc.* **2016**, *138*, 5159–5170. [CrossRef]
8. Ullah, I.; Taha, T.A.; Alenad, A.M.; Uddin, I.; Hayat, A.; Hayat, A.; Sohail, M.; Irfan, A.; Khan, J.; Palamanit, A. Platinum-Alumina Modified SO_4^{2-}-ZrO_2/Al_2O_3 Based Bifunctional Catalyst for Significantly Improved n -butane Isomerization Performance. *Surf. Interfaces* **2021**, *25*, 101227. [CrossRef]
9. Li, J.; Wu, N. Semiconductor-based photocatalysts and photoelectrochemical cells for solar fuel generation: A review. *Catal. Sci. Technol.* **2014**, *5*, 1360–1384. [CrossRef]
10. Cheng, H.; Huang, B.; Liu, Y.; Wang, Z.; Qin, X.; Zhang, X.; Dai, Y. An anion exchange approach to Bi_2WO_6 hollow microspheres with efficient visible light photocatalytic reduction of CO_2 to methanol. *Chem. Commun.* **2012**, *48*, 9729–9731. [CrossRef]
11. Liu, Q.; Zhou, Y.; Kou, J.; Chen, X.; Tian, Z.; Gao, J.; Yan, S.; Zou, Z. High-Yield Synthesis of Ultralong and Ultrathin Zn_2GeO_4 Nanoribbons toward Improved Photocatalytic Reduction of CO_2 into Renewable Hydrocarbon Fuel. *J. Am. Chem. Soc.* **2010**, *132*, 14385–14387. [CrossRef]
12. Liu, S.; Yu, J. Effect of F-Doping on the Photocatalytic Activity and Microstructures of Nanocrystalline TiO_2 Powders. *Nanostruct. Photocatal.* **2016**, 187–200. [CrossRef]

13. Ah, A.; Ns, B.; Skbm, C.; Ah, D.; Jk, E.; Aur, F.; Tl, G. Molecular engineering of polymeric carbon nitride based Donor-Acceptor conjugated copolymers for enhanced photocatalytic full water splitting. *J. Colloid Interface Sci.* **2020**, *560*, 743–754.
14. Lopez-Tenllado, F.J.; Murcia-López, S.; Gómez, D.M.; Marinas, A.; Marinas, J.M.; Urbano, F.J.; Navío, J.A.; Hidalgo, M.C.; Gatica, J.M. A comparative study of Bi_2WO_6, CeO_2, and TiO_2 as catalysts for selective photo-oxidation of alcohols to carbonyl compounds. *Appl. Catal. Gen. Int. J. Devoted Catal. Sci. Its Appl.* **2015**, *505*, 375–381.
15. Pare, B.; Singh, P.; Jonnalgadda, S. Degradation and mineralization of victoria blue B dye in a slurry photoreactor using advanced oxidation process. *J. Sci. Ind. Res.* **2009**, *68*, 724–729.
16. Khan, M.; Hayat, A.; Mane, S.; Li, T.; Khan, W.U. Functionalized nano diamond composites for photocatalytic hydrogen evolution and effective pollutant degradation. *Int. J. Hydrog. Energy* **2020**, *45*, 29070–29081. [CrossRef]
17. Sohail, M.; Xue, H.; Jiao, Q.; Li, H.; Khan, K.; Wang, S.; Zhao, Y. Synthesis of well-dispersed TiO_2@reduced graphene oxide (rGO) nanocomposites and their photocatalytic properties. *Mater. Res. Bull.* **2017**, *90*, 125–130. [CrossRef]
18. Hayat, A.; Rahman, M.U.; Khan, I.; Khan, J.; Sohail, M.; Yasmeen, H.; Liu, S.Y.; Qi, K.; Lv, W. Conjugated Electron Donor–Acceptor Hybrid Polymeric Carbon Nitride as a Photocatalyst for CO_2 Reduction. *Molecules* **2019**, *24*, 1779. [CrossRef]
19. Hayat, A.; Chen, Z.; Luo, Z.; Fang, Y.; Wang, X. π-deficient pyridine ring-incorporated carbon nitride polymers for photocatalytic H_2 evolution and CO_2 fixation. *Res. Chem. Intermed.* **2021**, *47*, 15–27. [CrossRef]
20. Kumar, A.; Raizada, P.; Thakur, V.K.; Saini, V.; Khan, A.A.P.; Singh, N.; Singh, P. An overview on polymeric carbon nitride assisted photocatalytic CO_2 reduction: Strategically manoeuvring solar to fuel conversion efficiency. *Chem. Eng. Sci.* **2021**, *230*, 116219. [CrossRef]
21. Hasija, V.; Sudhaik, A.; Raizada, P.; Hosseini-Bandegharaei, A.; Singh, P. Carbon quantum dots supported AgI/ZnO/phosphorus doped graphitic carbon nitride as Z-scheme photocatalyst for efficient photodegradation of 2,4-dinitrophenol. *J. Environ. Chem. Eng.* **2019**, *7*, 103272. [CrossRef]
22. Sudhaik, A.; Raizada, P.; Thakur, S.; Saini, R.V.; Saini, A.K.; Singh, P.; Thakur, V.K.; Nguyen, V.-H.; Khan, A.A.P.; Asiri, A.M. Synergistic photocatalytic mitigation of imidacloprid pesticide and antibacterial activity using carbon nanotube decorated phosphorus doped graphitic carbon nitride photocatalyst. *J. Taiwan Inst. Chem. Eng.* **2020**, *113*, 142–154. [CrossRef]
23. Mills, A.; Le Hunte, S. An overview of semiconductor photocatalysis. *J. Photochem. Photobiol. A Chem.* **1997**, *108*, 1–35. [CrossRef]
24. Widegren, J.A.; Finke, R.G. A review of the problem of distinguishing true homogeneous catalysis from soluble or other metal-particle heterogeneous catalysis under reducing conditions. *J. Mol. Catal. A Chem.* **2003**, *198*, 317–341. [CrossRef]
25. Belver, C.; Bedia, J.; Gómez-Avilés, A.; Peñas-Garzón, M.; Rodriguez, J.J. Semiconductor Photocatalysis for Water Purification. In *Nanoscale Materials in Water Purification*; Elsevier: Amsterdam, The Netherlands, 2019; pp. 581–651.
26. Zhang, F.; Wang, X.; Liu, H.; Liu, C.; Wan, Y.; Long, Y.; Cai, Z. Recent advances and applications of semiconductor photocatalytic technology. *Appl. Sci.* **2019**, *9*, 2489. [CrossRef]
27. Zhang, L.; Ran, J.; Qiao, S.-Z.; Jaroniec, M. Characterization of semiconductor photocatalysts. *Chem. Soc. Rev.* **2019**, *48*, 5184–5206. [CrossRef] [PubMed]
28. Xu, Y.; Schoonen, M.A. The absolute energy positions of conduction and valence bands of selected semiconducting minerals. *Am. Mineral.* **2000**, *85*, 543–556. [CrossRef]
29. Hayat, A.; Taha, T.A.; Alenad, A.M.; Ullah, I.; Shah, S.; Uddin, I.; Ullah, I.; Hayat, A.; Khan, W.U. A simplistic molecular agglomeration of carbon nitride for optimized photocatalytic performance. *Surf. Interfaces* **2021**, *25*, 101166. [CrossRef]
30. Hayat, A.; Sohail, M.; Taha, T.A.; Alenad, A.M.; Uddin, I.; Hayat, A.; Ali, T.; Shah, R.; Irfan, A.; Khan, W.U.; et al. A Superficial Intramolecular Alignment of Carbon Nitride through Conjugated Monomer for Optimized Photocatalytic CO_2 Reduction. *Catalysts* **2021**, *11*, 935. [CrossRef]
31. Raziq, F.; Hayat, A.; Humayun, M.; Mane, S.; Liang, Q. Photocatalytic solar fuel production and environmental remediation through experimental and DFT based research on CdSe-QDs-coupled P-doped-g-C_3N_4 composites. *Appl. Catal. B Environ.* **2020**, *270*, 118867. [CrossRef]
32. Hayat, A.; Alrowaili, Z.A.; Taha, T.A.; Khan, J.; Khan, W.U. Organic heterostructure modified carbon nitride as apprehension for Quercetin Biosensor. *Synth. Met.* **2021**. [CrossRef]
33. Hayat, A.; Raziq, F.; Khan, M.; Khan, J.; Khan, W.U. Fusion of conjugated bicyclic co-polymer within polymeric carbon nitride for high photocatalytic performance. *J. Colloid Interface Sci.* **2019**, *554*, 627–639. [CrossRef] [PubMed]
34. Hayat, A.; Raziq, F.; Khan, M.; Ullah, I.; Khan, W.U. Visible-light enhanced photocatalytic performance of Polypyrrole/g-C_3N_4 composites for water splitting to evolve H_2 and pollutants degradation. *J. Photochem. Photobiol. A Chem.* **2019**, *379*, 88–98. [CrossRef]
35. Huang, C.; Wen, Y.; Ma, J.; Dong, D.; Zhang, Y. Unraveling fundamental active units in carbon nitride for photocatalytic oxidation reactions. *Nat. Commun.* **2021**, *12*, 320. [CrossRef]
36. Hayat, A.; Taha, T.A.; Alenad, A.M.; Ali, T.; Bashir, T.; Rehman, A.U.; Ullah, I.; Hayat, A.; Irfan, A.; Khan, W.U. A molecular amalgamation of carbon nitride polymer as emphasized photocatalytic performance. *Int. J. Energy Res.* **2021**, *45*, 19921–19928. [CrossRef]
37. Ullah, A.; Khan, J.; Sohail, M.; Hayat, A.; Khan, W.U. Fabrication of Polymer Carbon Nitride with Organic Monomer for Effective Photocatalytic Hydrogen Evolution. *J. Photochem. Photobiol. A Chem.* **2020**, *401*, 112764. [CrossRef]
38. Khan, M.; Li, T.; Hayat, A.; Zada, A. A concise review on the elastomeric behavior of electroactive polymer materials. *Int. J. Energy Res.* **2021**. [CrossRef]

39. Ah, A.; Ns, B.; Iu, C.; Mk, D.; Skbmb, E.; Ah, F.; Iu, G.; Aur, H.; Ta, I.; Gm, J. Molecular engineering of carbon nitride towards photocatalytic H_2 evolution and dye degradation. *J. Colloid Interface Sci.* **2021**, *597*, 39–47.
40. Xu, J.; Gao, J.; Chao, W.; Yu, Y.; Lei, W. NH_2 -MIL-125(Ti)/graphitic carbon nitride heterostructure decorated with NiPd co-catalysts for efficient photocatalytic hydrogen production. *Appl. Catal. B Environ.* **2017**, *219*, 101–108. [CrossRef]
41. Arif, N.; Uddin, I.; Hayat, A.; Khan, W.U.; Ullah, S.; Hussain, M. Homogeneous Iron-Doped Carbon Nitride-Based Organo-catalysts for sensational photocatalytic performance under Visible Light-Driven. *Polym. Int.* **2021**, *70*, 1273–1281. [CrossRef]
42. Hayat, A.; Shaishta, N.; Mane, S.K.B.; Khan, J.; Hayat, A. Rational Ionothermal Copolymerization of TCNQ with PCN Semiconductor for Enhanced Photocatalytic Full Water Splitting. *ACS Appl. Mater. Interfaces* **2019**, *11*, 46756–46766. [CrossRef] [PubMed]
43. Rahman, M.U.; Hayat, A. Green synthesis, properties, and catalytic application of zeolite (P) in production of biofuels from bagasse. *Int. J. Energy Res.* **2019**, *43*, 4820–4827. [CrossRef]
44. Hayat, A.; Li, T. A facile supramolecular aggregation of trithiocyanuric acid with PCN for high photocatalytic hydrogen evolution from water splitting. *Int. J. Energy Res.* **2019**, *43*, 5479–5492. [CrossRef]
45. Nie, N.; Zhang, L.; Fu, J.; Cheng, B.; Yu, J. Self-assembled hierarchical direct Z-scheme g-C_3N_4/ZnO microspheres with enhanced photocatalytic CO_2 reduction performance. *Appl. Surf. Sci. J. Devoted Prop. Interfaces Relat. Synth. Behav. Mater.* **2018**, *441*, 12–22.
46. Zhu, W.; Ke, J.; Wang, S.B.; Ren, J.; Wang, H.H.; Zhou, Z.Y.; Si, R.; Zhang, Y.W.; Yan, C.H. Shaping Single-Crystalline Trimetallic Pt-Pd-Rh Nanocrystals toward High-Efficiency C–C Splitting of Ethanol in Conversion to CO_2. *ACS Catal.* **2015**, *5*, 1995–2008. [CrossRef]
47. Wang, Y.; Wang, X.; Antonietti, M. ChemInform Abstract: Polymeric Graphitic Carbon Nitride as a Heterogeneous Organocatalyst: From Photochemistry to Multipurpose Catalysis to Sustainable Chemistry. *ChemInform* **2012**, *43*. [CrossRef]
48. Lin, J.; Pan, Z.; Wang, X. Photochemical Reduction of CO_2 by Graphitic Carbon Nitride Polymers. *ACS Sustain. Chem. Eng.* **2014**, *2*, 353–358. [CrossRef]
49. Di, W.; Yang, J.; Zhang, Y.; Li, J.; Yu, Y.; Zhang, Y.; Zhu, Z.; Li, W.; Wu, C.; Luo, L. Device structure-dependent field-effect and photoresponse performances of p-type ZnTe:Sb nanoribbon. *J. Mater. Chem.* **2012**, *22*, 6206–6212.
50. Kibria, M.G.; Nguyen, H.; Cui, K.; Zhao, S.; Mi, Z. One-Step Overall Water Splitting under Visible Light Using Multiband InGaN/GaN Nanowire Heterostructures. *ACS Nano* **2013**, *7*, 7886–7893. [CrossRef] [PubMed]
51. Rehman, A.U.; Khan, M.; Zheng, M.; Khan, A.R.; Hayat, A. Thermochemical heat storage behavior of $ZnSO_4 \cdot 7H_2O$ under low-temperature. *Heat Mass Transf.* **2020**, *57*, 765–775. [CrossRef]
52. Nickel Oxide Nano-Particles on 3D Nickel Foam Substrate as a Non-Enzymatic Glucose Sensor. *J. Electrochem. Soc.* **2019**, *166*, B1602–B1611. [CrossRef]
53. Rehman, A.U.; Shah, M.Z.; Zhao, T.; Shah, R.; Zheng, M. Thermochemical heat storage ability of $ZnSO_4 \cdot 7H_2O$ as potential long-term heat storage material. *Int. J. Energy Res.* **2020**, *45*, 4746–4754. [CrossRef]
54. Shaishta, N.; Khan, W.U.; Mane, S.; Hayat, A.; Manjunatha, G. Red-emitting $CaSc_2O_4 : Eu^{3+}$ phosphor for NUV-based warm white LEDs: Structural elucidation and Hirshfeld surface analysis. *Int. J. Energy Res.* **2020**. [CrossRef]
55. Uddin, I.; Wang, G.; Gao, D.; Hussain, Z.; Hayat, A. Conventional and cement-catalyzed co-pyrolysis of rice straw and waste polyethylene into liquid and gaseous fuels by using a fixed bed reactor. *Biomass-Convers. Biorefinery* **2021**, 1–10. [CrossRef]
56. Jia, R.; Zhang, Y.; Yang, X. High efficiency photocatalytic CO_2 reduction realized by Ca^{2+} and HDMP group Co-modified graphitic carbon nitride. *Int. J. Hydrog. Energy* **2021**, *46*, 32893–32903. [CrossRef]
57. Fang, Y.; Fu, X.; Wang, X. Diverse polymeric carbon nitride-based semiconductors for photocatalysis and variations. *ACS Mater. Lett.* **2020**, *2*, 975–980. [CrossRef]
58. Sohail, M.; Xue, H.; Jiao, Q.; Li, H.; Khan, K.; Wang, S.; Feng, C.; Zhao, Y. Synthesis of well-dispersed TiO_2/CNTs@$CoFe_2O_4$ nanocomposites and their photocatalytic properties. *Mater. Res. Bull.* **2018**, *101*, 83–89. [CrossRef]